Tool Offset End-fly-cutting Method for Fabrication of Multi-boundary Lens Array

Guoqing Zhang (zhanggq@szu.edu.cn)
Shenzhen University https://orcid.org/0000-0003-0110-8614
Shuai Ma
Shenzhen University
Tong Luo
Shenzhen University
Jianpeng Wang
Shenzhen University
Jiankai Jiang
Shenzhen University

Original Article

Keywords: Slow tool servo, Micro structure, End-fly-cutting, Micro-lens array

Posted Date: October 25th, 2021

DOI: https://doi.org/10.21203/rs.3.rs-988548/v1

Title page

Tool offset end-fly-cutting method for fabrication of multi-boundary lens array

Guoqing Zhang, born in 1982, is currently an associate professor at *Shenzhen University, China*. He received his PhD degree from *The Hong Kong Polytechnic University, Hong Kong, China*, in 2014. His research interests include ultra-precision machining technology, robots and intelligent equipment.
Tel: +86-755-26536306; E-mail: zhanggq@szu.edu.cn

Shuai Ma, born in 1995, is currently a master candidate at *Shenzhen University, China*. His research interests include ultra-precision machining technology and intelligent equipment.
E-mail: 2070292081@szu.edu.cn

Tong Luo, born in 1995, is currently an engineer at *Sinopec Maoming Petrochemical Company, China*. He received his master degree from *Shenzhen University, China*, in 2021. His research interests include ultra-precision fly-cutting technology and equipment.
E-mail: luotong0947@163.com

Jianpeng Wang, born in 1996, is currently a master candidate at *Shenzhen University, China.* His research interests include ultra-precision machining technology and equipment.
E-mail: 1900291014@szu.edu.cn

Jiankai Jiang, born in 1995, is currently an engineer at *Sinopec Sales Co., Ltd. Guangdong Jiangmen Petroleum Branch, China*. He received his master degree from *Shenzhen University, China*, in 2021. His research interests include ultra-precision fly-cutting and equipment.
E-mail: 1834541113@qq.com

Corresponding author：Guoqing Zhang　E-mail：zhanggq@szu.edu.cn

ORIGINAL ARTICLE

Tool offset end-fly-cutting method for fabrication of multi-boundary lens array

Guoqing Zhang [1, 2] • Shuai Ma [1] • Tong Luo [1]• Jianpeng Wang [1]• Jiankai Jiang [1]

Received Oct xx, 202x; revised xx xx, 202x; accepted xx xx, 202x

Abstract: The lens arrays are widely used in advanced industrial fields such as national defense, medical care, and aerospace due to its special optical performance. Single-point diamond turning based on fast/slow tool servo technology is an important machining method to fabricate lens arrays. However, the constant-angle or constant-arc-length sampling of the spiral tool trajectory leads to the uneven distribution of surface data point cloud, which makes the theoretical morphology of microstructure deviate from their machined morphology, and seriously restricts the high precision, high flexibility and large-scale fabrication of the microstructure. This research provided a novel fabrication method for machining multi-boundary lens arrays by employing tool offset end-fly-cutting method which interchanged the position of the tool and workpiece, and a mathematical model was established to generate the uniform tool trajectory covering the multi-boundary lens array. Through the comparison of measured and simulated results, the root-mean-square (RMS) error of multi-boundary lens array's sectional curve is below 1 μm, proving the effectiveness of the machining method. This method provided a new technical scheme for the fabrication of multi-boundary lens arrays, and provided a theoretical reference for machining multi-scale microstructures.

Keywords: Slow tool servo • Micro structure • End-fly-cutting • Micro-lens array

✉ Guoqing Zhang
zhanggq@szu.edu.cn

[1] Shenzhen Key Laboratory of High Performance Nontraditional Manufacturing, College of Mechatronics and Control Engineering, Shenzhen University, Nan-hai Ave 3688, Shenzhen 518060, Guangdong, China

[2] Guangdong Key Laboratory of Electromagnetic Control and Intelligent Robots, College of Mechatronics and Control Engineering, Shenzhen University, Nan-hai Ave 3688, Shenzhen 518060, Guangdong, China

1 Introduction

Insect compound eyes have anti-fogging and high-wide imaging characteristics, and their corresponding bionic lens arrays are widely used in imaging, biosensing, medicine and other fields [1]. In order to fabricate the micro lens array with a high-quality surface, a mechanical physical removal method is usually used. For obtaining complex optical elements surfaces such as off-axis aspheric surfaces, toroidal surfaces, sinusoidal array structures, and Alvarez micro lens arrays [2, 3], the fast/slow tool servo turning, ultra-precision fly-cutting and other machining technologies have been developed [4, 5].

There are many practical studies and outstanding results on micro/nano structure surface machining, most of them focused on the machining method such as slow tool servo (STS), fast tool servo (FTS), and end-fly-cutting. The STS is suitable for machining smooth and continuous symmetrical surfaces, such as diffraction gratings, aspheric surfaces, lens arrays and composite microstructures [6, 7]. Neo et al. [8] proposed a machining technology for fabricating hexagonal Fresnel lens array based on STS technology. Huang et al. [9] designed an interactive movement of the tool and the workpiece, and directly machined the radial Fresnel lens structure on the roller mold. To et al. (2016) proposed a diamond turning method based on virtual spindle tool servo to fabricate the discontinuous structure of micro-optical array [10]. However, limited by the motion frequency of the STS, the rapid response of the lathe cannot be achieved for machining the high-curvature variety microstructure profile. The fast tool servo (FTS) has been developed correspondingly, which is not restricted by the lathe servo unit, therefore, the tool can obtain a high motion frequency [11, 12]. Neo et al. [13] proposed a surface analytical model to evaluate the cutting linearization error in FTS

machining freeform surfaces. Zhu et al. [14] proposed a new adaptive tool servo diamond turning technology to improve the machining accuracy by optimizing the machining path. Tong et al. [15] successfully generated microgrooves in Alvarez lens arrays, which improved the ability of FTS to machine multi-level structures.

The realization of micro/nano structure surface is based on the F/STS technology and the discretized tool trajectory data points [16]. In the turning process, with the tool feeding to the workpiece center, the cutting speed of the tool along the tangential direction decreases correspondingly. In F/STS machining, the constant-angle and constant-arc-length sampling method of tool position results in the inconsistent density of data point, and affects the machining surface quality finally. Therefore, in order to achieve large-scale and high-quality surface machining, ultra-precision fly-cutting technology has been proposed which is widely used in machining aluminum alloy flat mirrors and micro-groove structures [17], and this technology combined with F/STS to machine complex structure surfaces, such as freeform surfaces with micro/nano structures. Zhu et al. [18-20] based on four-axis ultra-precision lathe to fabricate large-scale micro-lens array by using the end fly-cutting servo method, and in favor of the remaining tool traces to build secondary nanostructures.

This research is based on the end-fly-cutting technology which the workpiece and the tool are interchanged to generate a circular arc path, and employed an innovative method of machining lens array based on the three-axis ultra-precision lathe. Firstly, a mathematical model for calculating tool position points under the tool arc path is established. Based on this model, the circular boundary, square boundary and hexagonal boundary lens array are fabricated respectively. Through the comparison of measured results and simulation results, the amplitude and distribution of machining errors are discussed. This method has uniform and average machining characteristics in the fabrication process, and solves the problem of inconsistent data point dispersion and gradual linear speed in F/STS. It is an effective process for large-scale fabricating of multi-boundary lens arrays and provides a theoretical and technical reference for the fabricating of complex micro/nano structures arrays.

2 Tool path and surface generation

The slow-tool servo system of the tool offset rotation path proposed in this paper is designed and developed on a commercial ultra-precision lathe, the lathe equipped only X, Z, and C axes. The system composition is shown in Figure 1 (a), the cutting tool is attached on the spindle through a fixture and rotates with it. The rotation of the spindle makes the machining path of the diamond tool changes from the traditional spiral trajectory to the uniformly arranged arc trajectory. The workpiece is fixed on the holder, and the Z-axis of the lathe drives it to perform reciprocating linear motion to realize the feed in the cutting depth direction, with the linkage of the C-axis and X-axis, the required micro/nano structure can be fabricated. The surface data point sampling method of the tool offset rotation path servo technology has greater advantages than the traditional F/STS technology. As shown in Figure 1 (b), the tool offset rotation path is more evenly distributed than the traditional spiral trajectory tool path, and the intervals between the data points on the tool path are equal. At the same time, under the constant rotation speed of the spindle, the linear speed of the tool rotation is also constant, which is beneficial to fabricate micro/nano structures uniformly.

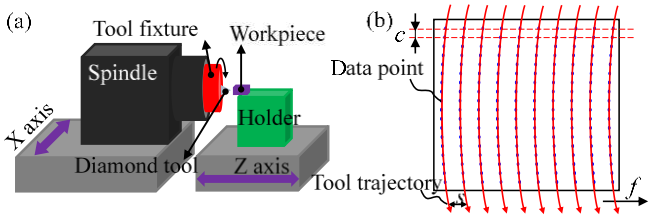

Figure 1 Schematic of (a) tool offset end-fly-cutting system and (b) sampling points of the rotating tool path

The lens array is mainly based on the arrangement of lens units to produce different performance, and their arrangement is shown in Figure. 2. By changing the relative distances h and w between the centers of adjacent lens units in Figure 2 (a), a lens array with a specific boundary can be combined and arranged, such as the square boundary lens array and the hexagonal boundary lens array shown in Figure 2 (c) and (d).

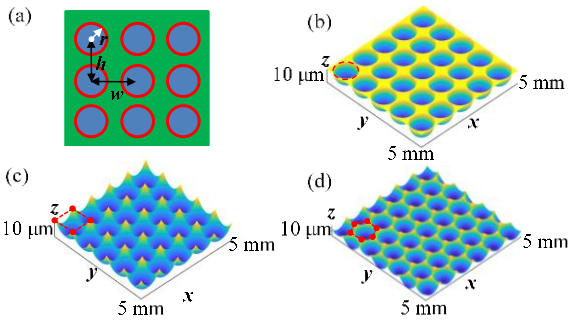

Figure 2 Simulation of three types of lens arrays (a) Arrangement of lens array; (b) Circular boundary lens array (h=2r, w=2r); (c) Square boundary lens array (h=r, w=r); (d)

Hexagonal boundary lens array (h=1.5r, w=$\sqrt{3}r$)

In order to obtain the lens array by the tool offset end-fly-cutting, it is necessary to perform theoretical calculation on the tool position and establish the mathematical model of tool path. Firstly, establish a rectangular machining area with length W and height H, this area needs to meet the condition that half of the height value is less than the rotation radius of diamond tool, otherwise a failure area will appear. The cutting edge of the diamond tool used by this mathematical model is arc-shaped and the rake angle is 0°. As shown in Figure 3 (a), a coordinate system $x_wo_wy_w$ at the middle of the left boundary line of the workpiece was established, and the lens array on the $x_wo_wy_w$ surface of the workpiece coordinate system was projected. Set the distance from the tool rotation center to the left boundary line of the workpiece as s, the rotation radius of the tool is R, the center point of the cutting edge arc is the tool position, and the center of tool rotation moves with the spindle to the positive direction of the x_w axis in the workpiece coordinate system. In order to realize the feed in the x direction of the three-axis lathe, the feed speed in the x-direction is set to f. Because the rake face of the tool always contacts the workpiece, it needs to pay attention to rotation direction of the spindle during machining. The rake face direction of the tool shown in Figure 3 (a) is downward, and it appears to rotate counterclockwise when projected to the workpiece coordinate system, at this time, the spindle rotates clockwise.

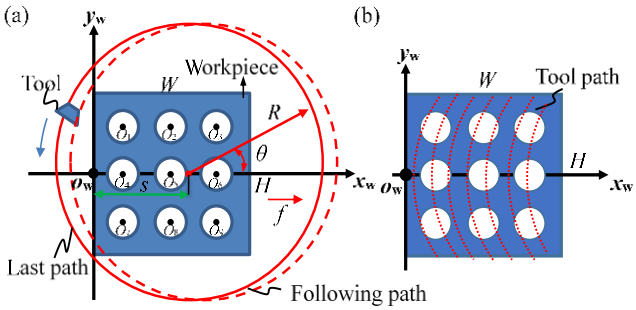

Figure 3 Schematic of (a) tool rotation and feed, and (b) tool path covering the lens array

In the process of machining the entire rectangular area, the spindle revolutions are defined as n, and each revolution arc is divided into l points with a constant angle. The current tool position defined as point k, then the coordinates (x_s, y_s) of the tool edge arc center projected on the workpiece coordinate system $x_wo_wy_w$ can be expressed by:

$$\begin{cases} x_s = R\times\cos(\theta)+n\times f+s \\ y_s = R\times\sin(\theta) \end{cases} \tag{1}$$

where $\theta = k\times\dfrac{2\pi}{l}$

According to the arc trajectory of the tool rotation, the tool points of the entire lens array are divided as shown in Figure 3 (b). The diamond tool will machine each lens unit evenly, therefore, one of the units is used to establish a mathematical model for calculating single tool position. For the lens unit O_1 shown in Figure 4, its radius is r, and the equation of circle boundary projected on the workpiece surface coordinate system $x_wo_wy_w$ is:

$$\left(x-x_{O_1}\right)^2+\left(y-y_{O_1}\right)^2=r^2 \tag{2}$$

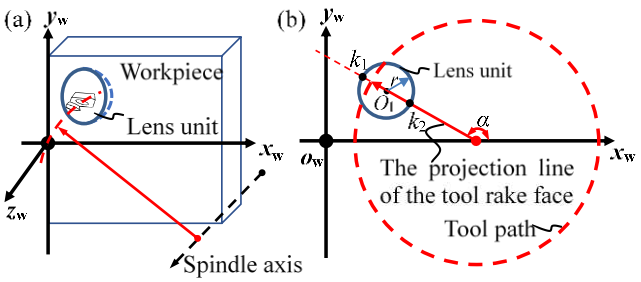

Figure 4 Schematic of (a) the lens unit formation in single tool path, and (b) the geometric relation between the projection line of tool rake face and tool path on $x_wo_wy_w$ coordinate plane

As shown in Figure 4, the rake angle of the diamond tool is set to 0°. When the tool position moves to the lens unit area, the plane of the rake face can intercept the unit lens to obtain a circular section, and the plane where the rake face is projected to the $x_wo_wy_w$ coordinate system is a straight line, which can be expressed as:

$$y=\tan\alpha\times x+n\times f-s \tag{3}$$

where the α equal to θ.

The projection of the tool position in the xoy coordinate system is on the ray emitted from the center of the coordinate system. In the real machining, affected by the machining accuracy of the fixture and the assembly accuracy of the installation, the tool position will change in the mathematical model, therefore the rake face needs to be compensated in the model. Supposing the actual tool height is h_d, the actual depth of the tool slot is h_w, an angle compensation is performed on the angle α and the actual

value of the compensation angle α' can be expressed as:

$$\alpha' = \alpha + \arcsin\left(\frac{h_w - h_d}{R}\right) \tag{4}$$

Substituting the angle α in Eq. (3) with the α', and combining Eq. (2) and Eq (3) simultaneously, two points $k_1(x_1, y_1)$ and $k_2(x_2, y_2)$ can be solved. These points are the boundary points of the current cross-sectional circle of the lens unit. Set the distance from the horizontal plane of the lens unit center to the surface of the workpiece is h_1, and establish the coordinate system of the cross-sectional circle with the boundary points, the radius of the cross-sectional circle corresponding to the current tool position can be calculated as:

$$r_{(n,k)} = \sqrt{h_1^2 + \frac{|k_1k_2|}{2}} \tag{5}$$

where $|k_1k_2| = \sqrt{(x_2 - x_1)^2 + (y_2 - y_1)^2}$

As shown in Figure 5 (a), the coordinate system $x_no_nz_n$ between the cutting depth direction and the feed direction is established for the lens unit, and the projection equation of the unit can be expressed as:

$$x_{(n,k)}^2 + \left(z_{(n,k)} - \mathrm{h}_1\right)^2 = r^2{}_{(n,k)} \tag{6}$$

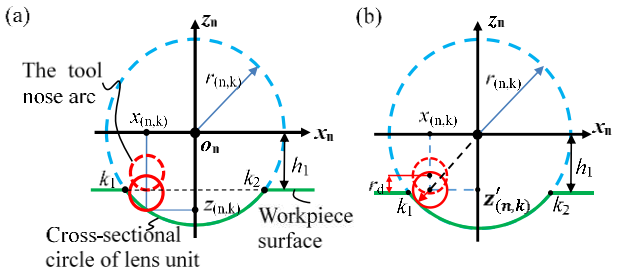

Figure 5 (a) Schematic of the interference between the rake face's tool nose arc and the lens unit's cross-sectional circle and its (b) compensation schematic

Based on the two points $k_1(x_1, y_1)$ and $k_2(x_2, y_2)$ calculated above, the tool position $x_{(n,k)}$ is expressed in the cross-section circular coordinate system as:

$$x_{(n,k)} = \sqrt{\left(x_s - x_1\right)^2 + \left(y_s - y_1\right)^2} - \frac{|k_1k_2|}{2} \tag{7}$$

Combined Eq. (6) and Eq. (7) can calculate the $z_{(n,k)}$, which is the current tool position feed value.

The tool nose arc cuts into the lens according to the z_n direction shown in Figure 5 (a), when the tool position is fed in the z direction, the tool nose arc overcuts the cross-sectional circle of the lens, therefore, interference compensation must be performed at this point. As shown in Figure 5 (b), the tool position in this coordinate system is expressed as:

$$z'_{(n,k)} = -\sqrt{\left(r_{(n,k)} - r_d\right)^2 - x_{(n,k)}^2} \tag{8}$$

Therefore, the specific value of the tool position of the workpiece coordinate system can be expressed as:

$$z_s = z'_{(n,k)} + h_1 \tag{9}$$

For the circular boundary lens arrays, square boundary lens arrays, and hexagonal boundary lens array, the main difference between them is the shape of boundary, the judgment criteria can be expressed as:

$$\left(x_n - x_{o,n}\right)^2 + \left(y_n - y_{o,n}\right)^2 \le r_n^2 \tag{10}$$

where x_n,y_n are the coordinates of the tool position in the lathe coordinate system, and $x_{o,n}$,$y_{o,n}$ are the center point of the lens unit.

The center position of the circular and the square lens unit was given by:

$$\begin{cases} x_{n,o} = r_1 + n_k \times \left[x_{n.k} / n_k\right] \\ y_{n,o} = r_1 + n_k \times \left[y_{n.k} / n_k\right] \end{cases} \tag{11}$$

where r_1 is the radius of the lens unit.

Moreover, the judgement criteria of the boundary of the hexagonal lens array can be expresses as:

$$\begin{cases} o_{n,o} = \left[\dfrac{y_{n.k}}{3 \times r_1} + 0.5\right] \\ m_{n,o} = \left[\dfrac{x_{n.k}}{2 \times \cos\left(\pi / 6\right) \times r_1} + 0.5\right] \end{cases} \tag{12}$$

$$\begin{cases} y_{n,k} > \dfrac{\sqrt{3}}{3}\times(x_{n,k}-2\times\cos\left(\dfrac{\pi}{6}\right)\times r_1\times m_{n,o})+r_1+3\times r_1\times o_{n,o} \\ y_{n,k} < \dfrac{\sqrt{3}}{3}\times(x_{n,k}-2\times\cos\left(\dfrac{\pi}{6}\right)\times r_1\times m_{n,o})-r_1+3\times r_1\times o_{n,o} \\ y_{n,k} > -\dfrac{\sqrt{3}}{3}\times(x_{n,k}-2\times\cos\left(\dfrac{\pi}{6}\right)\times r_1\times m_{n,o})+r_1+3\times r_1\times o_{n,o} \\ y_{n,k} < -\dfrac{\sqrt{3}}{3}\times(x_{n,k}-2\times\cos\left(\dfrac{\pi}{6}\right)\times r_1\times m_{n,o})-r_1+3\times r_1\times o_{n,o} \end{cases} \tag{13}$$

Then the tool position point corresponding to the center of the lens unit can be expresses as:

$$\begin{cases} x_{n,o} = l_1/2 + l_1\times\left[\dfrac{x_{n,k}}{l_1}\right] \\ y_{n,o} = l_2/2 + l_2\times\left[\dfrac{y_{n.k}}{l_2}+0.5\right] \end{cases} \tag{14}$$

where, l_1=2×cos(π/6)×r_1, l_2=3×r_1.

If the criteria of Eq. (13) is not satisfied, the tool position point corresponding to the center of the lens unit is expressed as:

$$\begin{cases} x_{n,o} = l_1\times\left[\dfrac{x_{n,k}}{l_1}\right] \\ y_{n,o} = l_2\times\left[\dfrac{y_{n.k}}{l_2}+0.5\right] \end{cases} \tag{15}$$

By Eqs. (10) ~ (15), the professional software MATLAB is used to calculate the tool position of each lens array, and obtain the tool position simulation diagram of each lens array as shown in Figure 6.

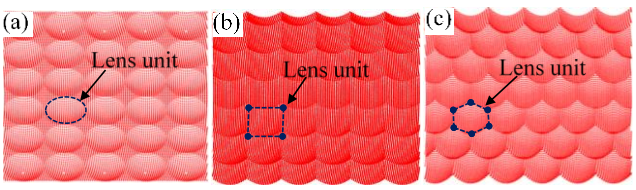

Figure 6 Data cloud of tool position to form lens array with (a) circle boundary, (b) square boundary and (c) hexagon boundary

3 Experiment and results analysis

3.1 Experiment setup

The machining experiment was performed on a three-axis CNC lathe (Moore Nanotech 450UPL) and its experiment setup was shown in the Figure 7 (a). In this machining system, the tool was fixed on the tool fixture and adsorbed in the spindle, the workpiece fixed on the tool holder, which is attached to the Z-axis, and the workpiece performs translational servo movement along the Z-axis. The PCD tool was used to obtain a roughly flat workpiece surface, and the diamond tool makes it smooth and manufactures the micro-lens array. Such microstructure was fabricated on the copper workpiece by controlling the rotation of the tool, the feed in the *x*-direction of the spindle and the reciprocating movement of the Z-axis. In this experiment, a diamond tool with the radius of 0.1 mm and the rake face of 0° was used, the speed of the spindle was set as 4 r/min, the rotating radius of the tool was 15 mm, and the maximum cutting depth of micro-lens array was 10 μm. The machined surface was then measured by Leica DM2700M optical microscope and Bruker Contour GT-X white light interferometer respectively, the measured result was then used for the surface quality and machining accuracy evaluation.

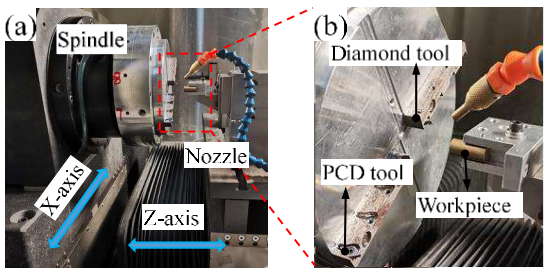

Figure 7 The experiment setup for (a) tool offset end-fly-cutting system based on X, Z, C three-axis lathe, and (b)the zoomed viewport in workpiece and tool

3.2 Results and discussion

The machined surface is shown in Figure. 8 (a)~(c). Observing the lens array under the optical microscope, each

unit is uniformly distributed and the shape of boundary is clear. The micro-lens array structure has good morphological characteristics which proves the correctness of the mathematical model and the effectiveness of the machining method. In order to obtain the surface parameters for specific analysis furtherly, the white light interferometer is used. The measured three-dimensional morphologies are shown in Figure 8 (d)~(f).

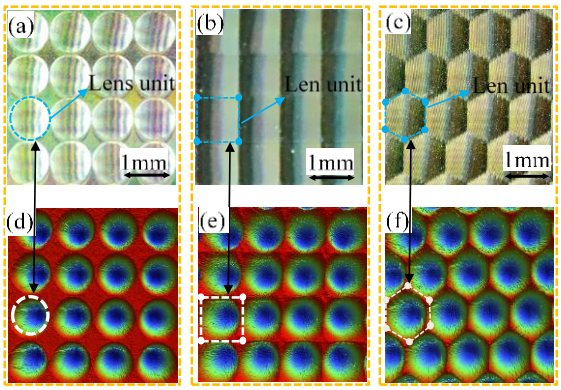

Figure 8 Morphologies of lens arrays with (a, d) circular boundary, (b, e) square boundary and (c, f) hexagon boundary (measured by Leica DM2700M optical microscope and Bruker Contour GT-X white light interferometer, respectively)

3.2.1 *Circular boundary lens array*

Figure 9 (a) and Figure 9 (b) show the three-dimensional morphological characteristics of the circular boundary lens array. The root mean square (RMS) is introduced to evaluate the curve error between the measured structure and the simulated structure. The calculation formula can be expressed as:

$$RMS = \sqrt{\frac{\sum_1^n (h_{sim} - h_{mea})^2}{n}} \tag{16}$$

The two-dimensional cross-sectional curve of the lens unit can be obtained along the *A*-*A*' direction and the *B*-*B*' direction, and the simulated curve of the lens unit can be calculated in the MATLAB. In order to analyze the morphological characteristics of the circular boundary lens array, the simulated curve is fitted with the measured cross-sectional curve, as shown in Figure 9 (c) and (d), the two curves have a great coincidence. Figure 9 (e) and (f) shows the form error, the RMS values in the horizontal and vertical axis directions are 0.6232 μm and 0.7576 μm respectively, and the overall form error value is less than 1 μm. There are many subtle fluctuations on the cross-sections curve, which are caused by residual burrs and material flow.

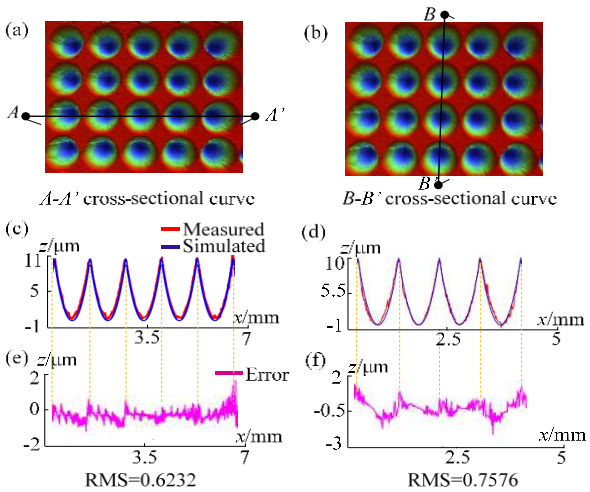

Figure 9 Three-dimensional morphology of circular boundary lens array and the position of (a) *A*-*A*' and (b) *B*-*B*' cross-sectional plane; comparison of the measured (c) *A*-*A'* and (d) *B*-*B'* cross-sectional curve with the simulated one; error curve for the cross-sectional curve on (e) *A*-*A'* and (f) *B*-*B'* section plane

3.2.2 *Square boundary lens array*

Figure 10 (a) and (b) show the three-dimensional morphological characteristics of the square boundary lens array. Fitting the simulated curve with the measured curve in *A*-*A*' and *B*-*B*' directions, as shown in Figure. 10 (c) and (d), the two curves have a highly overlap, the RMS values in the *A*-*A*' and *B*-*B*' directions are 0.2726 μm and 0.4688 μm respectively. The form error value is less than 1 μm. Due to the influence of burr remaining, the actual curve has obvious abrupt changes.

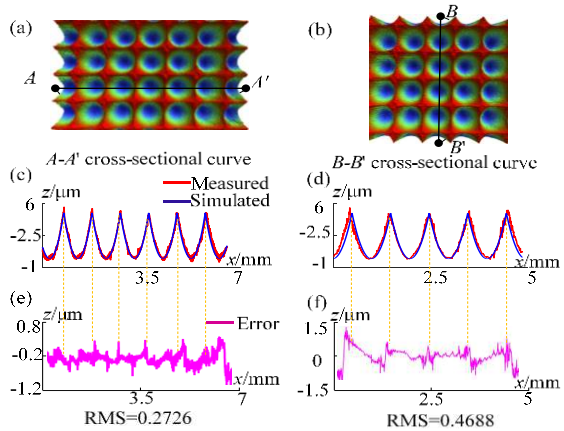

Figure 10 Three-dimensional morphology of square boundary lens array and the position of (a) *A*-*A*' and (b) *B*-*B*' cross-sectional plane; comparison of the measured (c) *A*-*A*' and (d) *B*-*B*' cross-sectional curve with the simulated one; error curve for the

cross-sectional curve on (e) *A*-*A*' and (f) *B*-*B*' section plane

3.2.3 *Hexagonal boundary lens array*

Figure 11 shows the three-dimensional morphological characteristics of the hexagonal boundary lens array. Getting the cross-sectional curve of the lens unit, then fit the simulated curve with the measured curve in the *A*-*A′* and *B*-*B′* directions, as shown in Figure 11 (c) and (d), the two curves has a great coincidence, the RMS value of the *A*-*A′* direction and the *B*-*B′* direction are 0.2726 μm and 0.5 μm respectively, and the overall form error value is less than 1 μm.

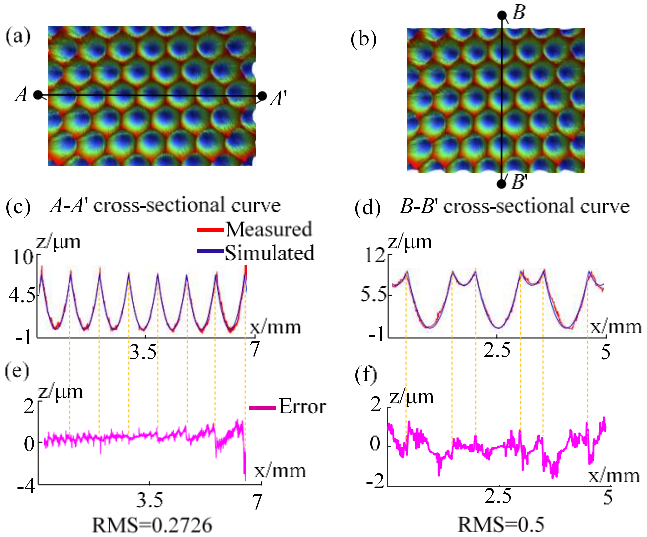

Figure 11 Three-dimensional morphology of hexagonal boundary lens array and the position of (a) *A*-*A′* and (b) *B*-*B*' cross-sectional plane; comparison of the measured (c) *A*-*A*' and (d) *B*-*B*' cross-sectional curve with the simulated one; error curve for the cross-sectional curve on (e) *A*-*A*' and (f) *B*-*B′* section plane

Through the analysis of the cross-sectional data of the three lens arrays, it can be found that the abrupt changes of the error are mainly concentrated on the boundary of the lens unit, and the interior of the lens unit has better fitting characteristics than the boundary of the lens. The reason is the previous lens unit will be squeezed by the cutting tool path of the next lens unit during the machining process, and the thickness of the boundary is thin, so the flow deformation occurs easily at the boundary, which increases the error.

5 Conclusions

This research proposed a machining method of multi-boundary lens array by tool offset end-fly-cutting, and established a mathematical model of the tool position. The main conclusions are as follows:

(1) The data point distribution of the tool arc trajectory takes into account the characteristics of constant-arc-length and constant-angles, and the linear speed remains constant during the machining process, which is conducive to fabricate micro/nano structures.

(2) The accuracy of positioning and machining can be improved by an offset method which was calculated in the current tool position.

(3) Performed surface simulation and machining experiments on the multi-boundary lens array structure, and compared the measured data with the simulated data of the surface, the root mean square error of the cross-sectional curve of the lens array is below 1 μm, which confirmed the effectiveness of the machining method.

(4) Large-scale and low-curvature variety surfaces can be machined by the proposed method compared with the traditional F/STS machining method, it also provided technical and theoretical references for fabricating other micro/nano structures.

6 Declaration

Acknowledgements

The work described in this paper was supported by the National Natural Science Foundation of China (Grant No. U2013603, 51827901), and the Shenzhen Natural Science Foundation University Stability Support Project (Grant No. 20200826160002001).

Availability of data and materials

The datasets supporting the conclusions of this article are included within the article.

Authors' contributions

The author' contributions are as follows: Guoqing Zhang was in charge of the whole trial; Shuai Ma and Tong Luo wrote the manuscript; Jiankai Jiang and Wang Jiangpeng assisted with sampling and laboratory analyses.

Competing interests

The authors declare no competing financial interests.

Consent for publication

Not applicable

Ethics approval and consent to participate

Not applicable

References

[1] Zhang L, Zhou L, Zhou W, Zhang S, Yi AY. Design, fabrication and testing of a compact large-field-of-view infrared compound eye imaging system by precision glass molding. *Precision Engineering*. 2020;66:87-98.

[2] Huang C, Li L, Yi AY. Design and fabrication of a micro Alvarez lens array with a variable focal length. *Microsystem Technologies*. 2008;15:559-63.

[3] Li LK, Yi AY. Design and fabrication of a freeform microlens array for uniform beam shaping. Microsystem *Technologies-Micro-and Nanosystems-Information Storage and Processing Systems*. 2011;17:1713-20.

[4] Zhang SJ, Zhou YP, Zhang HJ, Xiong ZW, To S. Advances in ultra-precision machining of micro-structured functional surfaces and their typical applications. *International Journal of Machine Tools & Manufacture*. 2019;142:16-41.

[5] Kong LB, Cheung CF, Lee WB. A theoretical and experimental investigation of orthogonal slow tool servo machining of wavy microstructured patterns on precision rollers. *Precision Engineering*. 2016;43:315-27..

[6] Takeuchi Y, Maeda S, Kawai T, Sawada K. Manufacture of multiple-focus micro Fresnel lenses by means of nonrotational diamond grooving. *Cirp Annals*. 2002;51:343-6.

[7] Li LH, Chan CY, Lee WB, Liu YH. A novel evaluation and compensation method for ultra-precision machining of hybrid lens. *Precision Engineering*. 2016;43:10-23.

[8] Neo DWK, Kumar AS, Rahman M. An automated Guilloche machining technique for the fabrication of polygonal Fresnel lens array. *Precision Engineering*. 2015;41:55-62.

[9] Huang R, Zhang XQ, Rahman M, Kumar AS, Liu K. Ultra-precision machining of radial Fresnel lens on roller moulds. *Cirp Annals*. 2015;64:121-4.

[10] To S, Zhu ZW, Wang HT. Virtual spindle based tool servo diamond turning of discontinuously structured microoptics arrays. *Cirp Annals*. 2016;65:475-8.

[11] Zhou M, Zhang HJ, Chen SJ. Study on Diamond Cutting of Nonrationally Symmetric Microstructured Surfaces with Fast Tool Servo. *Materials and Manufacturing Processes*. 2010;25:488-94.

[12] Zhu WL, Yang X, Duan F, Zhu Z, Ju B-F. Design and Adaptive Terminal Sliding Mode Control of a Fast Tool Servo System for Diamond Machining of Freeform Surfaces. *IEEE Transactions on Industrial Electronics*. 2019;66:4912-22.

[13] Neo DWK, Kumar AS, Rahman M. A novel surface analytical model for cutting linearization error in fast tool/slow slide servo diamond turning. *Precision Engineering*. 2014;38:849-60.

[14] Zhu Z, To S. Adaptive tool servo diamond turning for enhancing machining efficiency and surface quality of freeform optics. *Optics Express*. 2015;23:20234-48.

[15] Tong Z, Zhong WB, To S, Zeng WH. Fast-tool-servo micro-grooving freeform surfaces with embedded metrology. *Cirp Annals*. 2020;69:505-8.

[16] Li Z, Fang F, Zhang X, Liu X, Gao H. Highly efficient machining of non-circular freeform optics using fast tool servo assisted ultra-precision turning. *Optics Express*. 2017;25:25243-56.

[17] Zhu WL, Yang S, Ju BF, Jiang J, Sun A. Scanning tunneling microscopy-based on-machine measurement for diamond fly cutting of micro-structured surfaces. *Precision Engineering*. 2016;43:308-14.

[18] Zhu Z, To S, Zhang S. Large-scale fabrication of micro-lens array by novel end-fly-cutting-servo diamond machining. *Optics Express*. 2015;23:20593-604.

[19] To S, Zhu Z, Zeng W. Novel end-fly-cutting-servo system for deterministic generation of hierarchical micro–nanostructures. *Cirp Annals*. 2015;64:133-6.

[20] Zhu ZW, To S, Zhang SJ, Zhou XQ. High-Throughput Generation of Hierarchical Micro/Nanostructures by Spatial Vibration-Assisted Diamond Cutting. *Advanced Materials Interfaces*. 2016;3:1500477.

Biographical notes

Guoqing Zhang, born in 1982, is currently an associate professor at *Shenzhen University, China*. He received his PhD degree from *The Hong Kong Polytechnic University, Hong Kong, China*, in 2014. His research interests include ultra-precision machining technology, robots and intelligent equipment.
Tel: +86-755-26536306; E-mail: zhanggq@szu.edu.cn.

Shuai Ma, born in 1995, is currently a master candidate at *Shenzhen University, China*. His research interests include ultra-precision machining technology.
E-mail: 2070292081@szu.edu.cn.

Tong Luo, born in 1995, is currently an engineer at *Sinopec Maoming Petrochemical Company, China*. He received his master degree from *Shenzhen University, China*, in 2021. His research interests include ultra-precision fly-cutting technology and equipment.
E-mail: luotong0947@163.com

Jianpeng Wang, born in 1996, is currently a master candidate at *Shenzhen University, China.* His research interests include ultra-precision machining technology and equipment.
E-mail: 1900291014@szu.edu.cn

Jiankai Jiang, born in 1995, is currently an engineer at *Sinopec Sales Co., Ltd. Guangdong Jiangmen Petroleum Branch, China*. He received his master degree from *Shenzhen University, China*, in 2021. His research interests include ultra-precision fly-cutting technology and equipment.
E-mail: 1834541113@qq.com.